Versatile Direct Laser Writing Lithography Technique for Surface Enhanced Infrared Spectroscopy Sensors

Avi Braun[*], Stefan Alexander Maier

Blackett Laboratory, Department of Physics, Imperial College London, London SW7 2AZ, United Kingdom.

E-mail: a.braun@imperial.ac.uk

Abstract

A challenge for design, testing and fabrication of nano-structured chemical sensors is the fabrication of mm^2 size arrays of nano-structures in a reasonable time. Herein, we introduce and show how direct laser writing (DLW) in positive-tone photo-resists, followed by lift-off process can be used for fast fabrication (up to three-times faster than comparable Electron Beam lithography system) of arrays of nano-scale plasmonic structures with a great level of control over the design and dimensions of the nano-structures. We demonstrate the function of nano-structured arrays, fabricated by various DLW approaches, with surface enhanced infra-red absorption (SEIRA) detection of nine vibrational modes of PMMA. We also discuss the tunability of the plasmonic resonance – and hence the spectral detection range – by alteration of the size and array parameters of the nanostructures, and demonstrate the flexibility of this fabrication method by showing devices made of various substrate and antennas materials.

Keywords

Chemical detection, SEIRA , Plasmonic sensors, Direct laser writing, Nano-fabrication

When adsorbed near or on nano-structured metal surfaces, molecules can demonstrate a remarkable change in their optical properties with applications in surface enhanced spectroscopies. Two notable examples for such detection methods are surface enhanced Raman scattering (SERS)[1–4], and surface enhanced infrared absorption (SEIRA)[4–16]. In SEIRA spectroscopy, metallic and dielectric nano-antennas that exhibit plasmonic resonances in the Infra-Red (IR) regime are used to intensify the IR absorption signal of known vibrational modes of molecules, so that even small amount of analytes can be identified [4–16]. The improved detection originates from the excitation of localized surface plasmon resonances (LSPRs) – charge oscillations on the surface of the nano-structured surface – which give rise to a strong local electric field at the vicinity of the nanostructures and enhanced coupling between the textured surface and the vibrational modes of the adsorbed molecules. The enhancement is strongest when the plasmonic resonance of the nano-structures matches the spectral position of the vibrational fingerprints. This implies that that the spectral range at which improved detection is possible and the enhancement factor of the chemical sensor depend on sensor materials [12,15,16] (both of the nano-structures and the substrate), and the shape [13,14,17–19] and dimensions of individual structures[8,12,16,18] and the spacing between them [10].

---

[*] To whom correspondence should be addressed

Over the years different methods for patterning the nano textured surfaces have been developed, distinguished one from another by: size of the smallest attainable features and resolution, fabrication speed, level of control over the placement of the nanostructures, cost, and materials compatibility. For example, random distribution of nano-structures – typically by means of colloidal nano-particles (NP) – is a fast and low cost method for patterning large surfaces, albeit with minimal control over the positioning of the structures. On the other hand, Electron-Beam Lithography (EBL), accompanied by either lift-off, or etching/milling techniques, provides a flexible method for mask-less nano-patterning with nanometre resolution of practically any desirable 2D structures and array forms, but at high running costs and long writing times. Other fabrication methods that combine relatively-high throughput with some control over the position and shape of the nano-structures include: Laser Interference lithography[15], Nano-spherical-lens-lithography[20], hole–mask colloidal lithography[21], and nano-stencil lithography[22].

A Two-Photon Polymerization (TPP) direct laser writing (DLW) technique[16,23,24] has been demonstrated recently as a fast route for fabricating multi-millimetres arrays of nano-antennas for sensing applications in the IR spectral region, with an ultimate flexibility in structures design and fast writing speed. For example, Bagheri et. al.[16] demonstrated how DLW can be utilized to fabricate multi-mm size arrays of nano-structures on CaF_2 substrates for SEIRA spectroscopy with a top-down approach: first, a flat film, made from the antennas material is deposited on the substrate; then, DLW is used to cross-link a negative photo-resist dropped on top of the film, creating a hard mask with nano-meter features; the process is completed with selective carving of the antennas by means of ion-etching or ion-milling processes, followed by additional plasma-etching step to remove the hardened resist mask. Compared to the fabrication methods listed above, like EBL, DLW benefits from practically ultimate freedom in the positioning and the design of the shape of the nano-structures: it obviates the need for manufacturing of pre-defined masks (which are required for stencil lithography and UV photolithography), and the resulted nano-structures are independent of the size of the spheres as in the case of colloidal and spherical-lens lithography. With recently emerged new designs of SEIRA nano-structures which depart from simple bar-shaped antennas, the introduction of a flexible and fast fabrication method that can serve as an alternative to EBL is of great interest[13,14,17–19].

In this work we report the fabrication and testing of SEIRA chemical sensor based on an alternative approach for using TPP-DLW to fabricate large arrays of nano-structures. Here, the nano-structures are made by DLW followed by deposition of the antennas' materials and lift-off process, which enable fast and flexible fabrication method of plasmonic sensors that, in compare with the top-down approach, require less fabrication steps and obviating the need for additional etching/plasma equipment. In addition, in the method presented here, the same process can be used for the patterning of various materials, as opposed to methods which involve etching, as these have to be modified for each material in order to match the etching gas and/or the etching rate to the physical and chemical resistance of the etched material. The fabrication method discussed in this paper can be used also for other IR plasmonics[25], photonics and sensing applications[2,7] where sub-micron metallic or dielectric structures at the order of hundreds of nano-meters are needed.

We start by exploring three different TPP-DLW writing configurations and presenting examples of arrays of nano-antennas fabricated by these methods, followed by optical measurements and analysis of the mid-IR resonances and the enhanced reflection spectra of thin film of Polymethyl methacrylate (PMMA) on arrays of Au antennas of different sizes and longitudinal and transversal spacing. We show that with a careful design of the nano-structures our sensors can optically reveal the fingerprints of nine different molecular vibrations, most of which are practically invisible for planar surfaces, and others with an enhancement factor of more than 20. Finally, we demonstrate the versatility of this fabrication method by presenting arrays of structures made of different materials by TPP-DLW combined with the lift-off process.

Experimental section:

Sample preparation and direct laser writing

Prior to the writing process, borosilicate glass and Si substrates were cleaned with Acteon, bi-propanol, and de-ionised water in an ultrasonic bath, and dried with N_2. For the photoresist layer, a high precision positive-tone resist (AZ 701 MiR, AZ Electronic Materials) was first diluted in Propylene Glycol Monomethyl Ether Acetate (PGMEA) at a volumetric ratio of 1.5:1 (AZ 701:PGMEA), and then spin coated on the substrates (30s at 3000 RPM), and soft baked on a hot plate (70s at 90°C) to form a uniform ~300 nm thick layer.

DLW was performed using a commercial Photonic Professional GT system (manufactured by Nanoscribe) equipped with a 780nm femto-second laser, and inverted microscope with a pair of objectives: 63X immersion-oil, and 20X air lens. Writing of arrays of antennas was done by deflecting (in a 2D horizontal plane) the laser light beam using the system's computer-controlled galvo mirrors; the system's motorized stage was used to write arrays larger than the galvo mirrors write field (200μm and 700μm in diameter for the 63X and 20X objectives, respectively). When using the 63X immersion objective, with a voxel length that is comparable to the thickness of the resist layer, each 2D antenna array was written three times at different planes (vertically spaced by 0.25μm) in order to ensure that the resist is fully exposed throughout its whole thickness. Movement along the vertical z-axis was done using the system's piezoelectric stage. After writing, samples were immersed for 30 seconds in TMAH based developer (MF26A, MEGAPOSIT), followed by a 10 seconds dip in DIW bath and N_2 dry.

Thin film deposition and lift off

A top-bench DC sputtering system (Q150T, Quorum Technologies) was used for sputtering of Gold (99.999%, Testbourne), Ti (99.995%, Testbourne), and ITO (In_2O_3/SnO_2 90-10 wt%, 99.99%, Testbourne). Thermal evaporation of Silver (99.99%, Sigma-Aldrich) and gold pellets (99.99%, Sigma-Aldrich), and Chromium plated tungsten rods (Kurt J. Lesker) was completed by an Åmod thermal evaporator (Angstrom Engineering). Gold nano-structures were deposited on top of a 3.5nm Ti, or 2.5nm Cr layer (for the sputtering and thermal evaporation processes, respectively) which served as adhesion layers. The fabrication process was completed by lifting-off the photoresist in Acetone (5 minutes at room temperature).

Measurements

The actual dimensions of the fabricated structures were measured using scanning electron microscope (eLINE, Raith). Reflection measurements were taken using an FTIR system with attached microscope (Hyperion series, Bruker cooperation). The mid-IR radiation was polarized using ZnSe holographic wire grid polarizer, and the reflected light was detected by a high sensitivity Hg-Cd-Te (MCT) Nitrogen cooled detector. During measurements the samples chamber was purged with dry air to reduce IR absorption by water molecules in the air.

Writing configurations

In this work we explored three DLW writing configurations. In the 'through substrate' configuration (Fig. 1a), a 170μm thick borosilicate glass is used as a substrate, through which the laser beam is focused into the photoresist layer using a 63X immersion-oil objective lens with a numerical aperture (NA) of 1.4. The index-matched optical path (from the objective to the photoresist, via the substrate) in this configuration, and the high NA of the immersion objective provide a sub micrometer-long voxel (along the vertical z-axis) with a diameter of ~300nm (in the x-y plane). However, while optically optimized, this approach can be utilized only for thin, transparent substrates that are optically matched

to the immersion objective. Alternative writing configurations that can be used for thick opaque substrates are shown in figures 1b and 1c. In the 'Non-contact' configuration (Fig. 1b), a 20X air objective (NA=0.5, with a working distance of 2.1mm) is used to directly expose the photo-resist. This versatile and straight-forward approach is easy to implement, albeit with a relatively low resolution and typical voxel length of 8μm and a diameter of 700-800nm due to the relatively low NA of the optical system. In the third alternative (Fig. 1c), the photoresist layer is span on the substrate (which may be opaque) and then temporarily mechanically attached to a glass coverslip, through which the resist is exposed. The coverslip allows exposing the resist using high NA immersion objective while keeping the photoresist clean and dry from oil or water. The performance of the 'through-coverslip' is expected to be modestly inferior to that of the 'through-glass' option due to apparent small air gaps at the interface of the photoresist and the coverslip. The writing speed and laser power for the three writing configurations were: 3mm/s and 14mW for the 'Through substrate' writing; 1mm/s and 33mW for the 20X air 'Non-Contact' method on glass substrate; and 1mm/s and 38mW when writing with the 'Through-coverslip' approach on Si substrates. The post writing process – chemical development of the resist, material deposition and chemical lift-off – is illustrated in figure 1d.
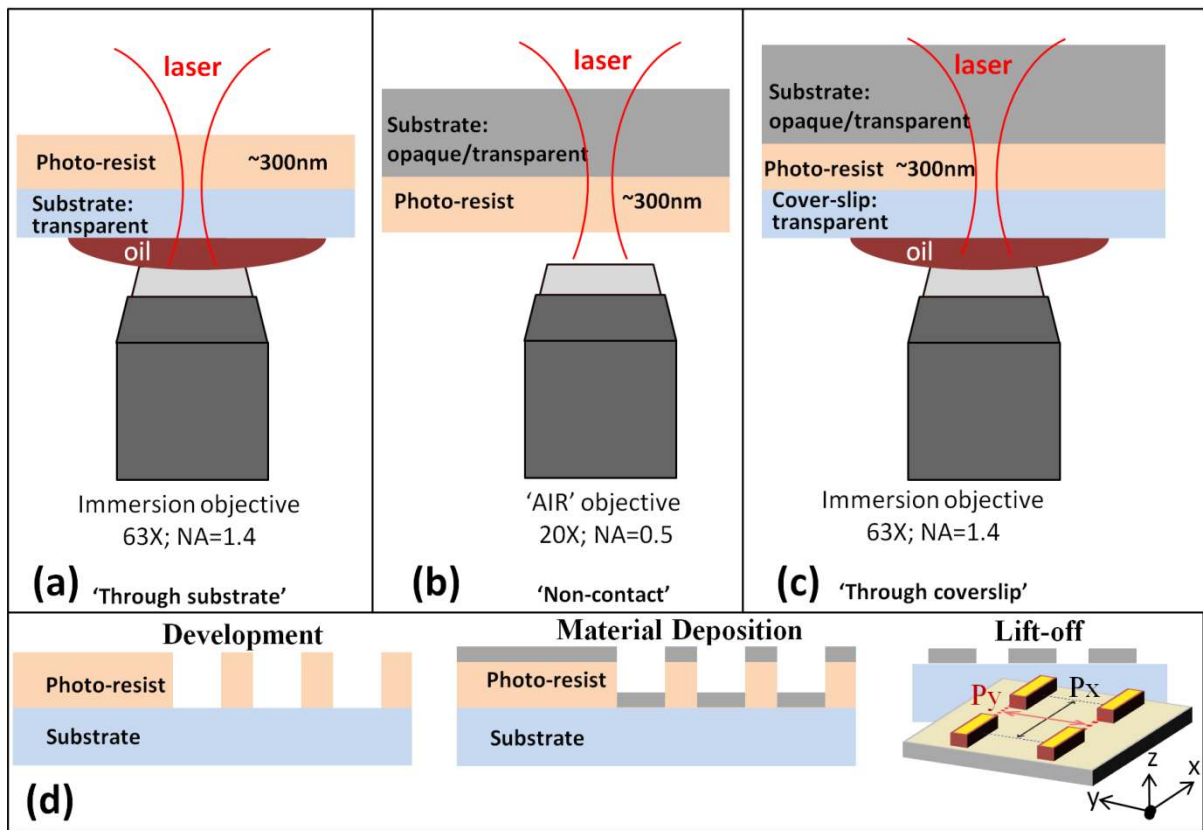

Figure 1. Schematic illustration (not to scale) of direct-laser-writing configurations and lift-off process. a) 'Through substrate' writing: the photoresist is spun on a transparent substrate; the laser beam is focused on the resist through the transparent substrate using an indexed matched immersion objective. b) 'Non-contact' writing: the laser beam is focused directly without any intermediate substance on the resist using an 'air' objective. c) 'Through-coverslip': a transparent coverslip is placed on top of the substrate and the resist to section between the immersion fluid and the photoresist; the laser beam is focused through the cover slip using an immersion objective. d) The lift off process (from left to right): after writing, the resist is developed and a thin film of material is deposited by means of thermal evaporation/sputtering. Finally, the resist is lifted off, resulting with arrays of nano-structures with the positive image of the laser writing. Px and Py in the inset represent the array periodicity along, and transverse the antennas, respectively.

Results and Discussion

Fabrication of nano-antennas. Arrays of 80x80μm 50nm thick Au nano-antennas were fabricated in each of the three configuration discussed above, with antennas length varied between L=1.0 to L=3.25 and arrays periodicity spanning between: Px=L+0.55 to L+1.35μm along the long axis antennas, and Py=1.2 to Py=2.0μm transverse the antennas. In total, up to 81 variants of antennas has been fabricated in each of the three configurations, covering between 7.5% to 22.5% of the substrate area. Examples of SEM images of selected arrays written with the three configurations are shown in Figure 2. With the exposures parameters given above, we reproducibly attained minimal antennas widths of 430, 750, and 460 nm for the 'Through substrate', 'Non-contact', and 'Through cover-slip' configurations, regardless of antennas length. The antennas fabricated with the high NA methods are comparable in size to those achieved by other 'fast-writing' techniques used for mid-IR plasmonic application, such as 'laser interference lithography'[15] and top-down direct laser writing[16]. For antennas written using the 63X objective, we found that in order to ensure that the ~300 nm resist is fully exposed throughout its whole thickness over the whole area of the arrays, each antenna had to be written multiple times at different planes separated by 0.2-0.3μm one from each other to balance any undesirable tilt of the sample: three layers were required for 80x80μm arrays written at a dose level just above the polymerization threshold, where one or two layers were sufficient for writing at higher doses. When writing with the 20X air objective, a single writing layer was sufficient thanks to its relatively long (~8μm) voxel. As the width of the polymerized resist depends on the exposure dose, we were able to gain a further control on the dimensions of the written structures by modifying the writing laser power: lower exposure doses produced structures with typical width 20-30% narrower than those stated above, but at lower yields (i.e. partial arrays with missing antennas, and great sensitivity to focusing); following the same trend, higher doses yielded wider antennas (e.g., increasing the laser intensity from 14mW to 27mW increased the width of the antennas from 430 to 600nm for the 'Through substrate' writing; writing at laser power of 50mW using the 'non-contact' method with the 20X objective yielded 950nm wide antennas). For the 'Through substrate' approach, antennas with similar dimensions were obtained also for higher laser power and writing speeds – 28mW and 12mm/s, respectively – in agreement with the known relation between the degree of polymerization of the resist and the laser intensity and writing speed parameters[24]: polymerization width $\propto laser\ intensity \cdot (writing\ speed)^{-0.5}$.
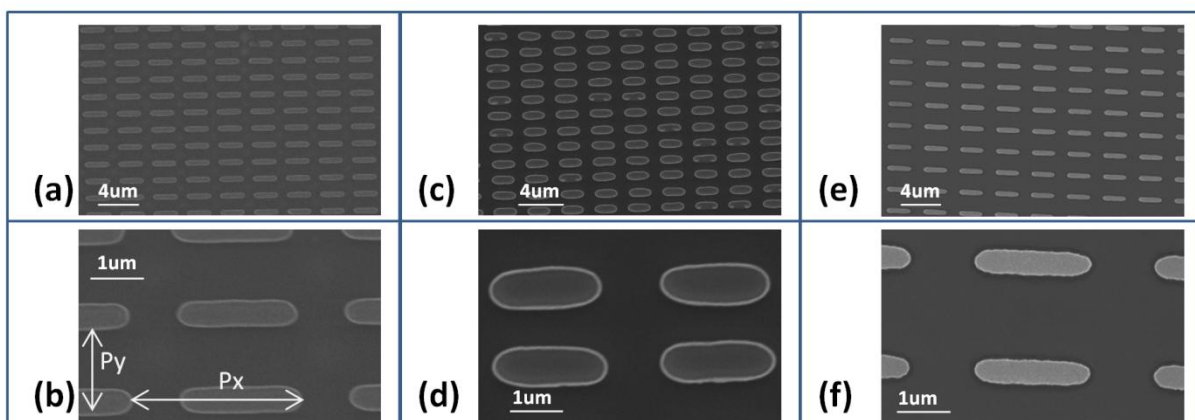

Figure 2: Scanning Electron Microscope images of 50nm high Au nano antennas. a-b) 'Through substrate' writing (fig. 1a) of gold sputtered arrays with antennas length of L=2.25μm ,and pitch distance along and transverse the antennas of Px=3.2μm and Py =1.6μm, respectively. c-d) 'Non contact' writing (fig. 1b) with the 20X air objective of L=2.1μm, Px=3.2μm and Py =1.5μm gold sputtered antennas. e-f) 'Through coverslip' writing (fig. 1c) of L=2.2μm, Px=3.4μm and Py =2.0μm thermally evaporated antennas on Si substrate.

Optical measurements. Infra-red reflection spectra (shown in absolute values) of sparsely spaced (Px=L+1.35μm, Py=2.0μm) Au nano-antennas arrays written on glass substrate using the 'through substrate' approach are shown in figure 3. When probed with light with electrical-field polarized along the *narrow* dimension of the antennas ('P90'; fig 3a), the reflectance curve is practically flat for wave-numbers smaller than 1600 [cm^{-1}], and is governed by the optical properties of the glass substrate, which is characterized by strong reflections for wave-number below 1250 [cm^{-1}] (equivalent to wavelength λ>8μm) and reduced reflectance at the spectral range between 1600 to 1250 [cm^{-1}] (see inset in figure 3a). Polarized light with the electrical field parallel to antennas' long axis ('P0'; fig 3b), on the other hand, induces plasmonic resonances in the metallic antennas, apparent in the form of distinct peaks in the reflection spectra with a maximum reflection wavelength that are increasing with antenna length. The effect of the dispersive nature of the glass substrates is apparent for wave-numbers below 1600 [cm^{-1}]. Despite the relatively low density of the antennas in this case (covering 7.5% to 12.5% of the total area for L=1.0μm to L=3.25μm), the absolute magnitude of the reflection signal reaches 70% for long antennas – an evidence to a scattering cross-section extending beyond the physical size of the nano-structures[8].
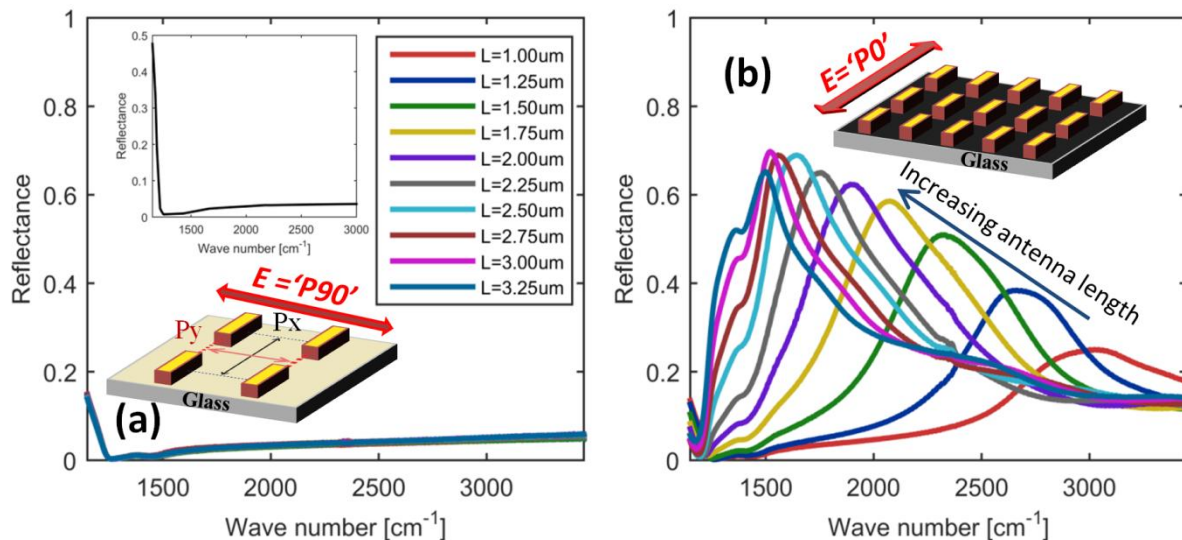

Figure 3: FTIR reflection measurements of Au antennas arrays, normalized relative to the reflectivity of gold coated glass substrate. The pitch distances along and transverse the antennas were Px=L+1.35μm and Py =2.0μm, respectively. a) Reflection spectra for IR light with the electrical field polarized along the *short* axis of the antennas ('P90'; represented by the red arrow in the inset), for antennas with lengths varying from 1.0 to 3.25μm. The calculated Fresnel reflection of glass (with optical constant taken from[26]) is shown in the inset. b) The same arrays probed with light polarized along the *long* axis of the antennas ('P0').

The resonance dependence on the length of the nano-antennas is summarized in figure 4a. For antenna length of 1 to ~2.5μm, the resonance wavelength increases linearly with the length of the antennas [10,27]. For longer structures, a sub-linear dependence is observed, and is associated with the glass substrate which alters the shape of the reflectance curve of the nano-arrays at λ>6μm (equivalent to ~1600 [cm^{-1}]) as discussed above. For closely packed arrays (fig. 4b) longitudinal and transverse dipolar coupling between neighboring antennas blue-shift and broaden the resonance peak[10,12] and introduce higher resonance orders. The broad range of tunability of antennas resonance by the engineering of antenna length and array spacing benefits SEIRA and other sensing applications where the resonance wavelength should be matched the wavelength of the vibrational mode of the sensed molecule.
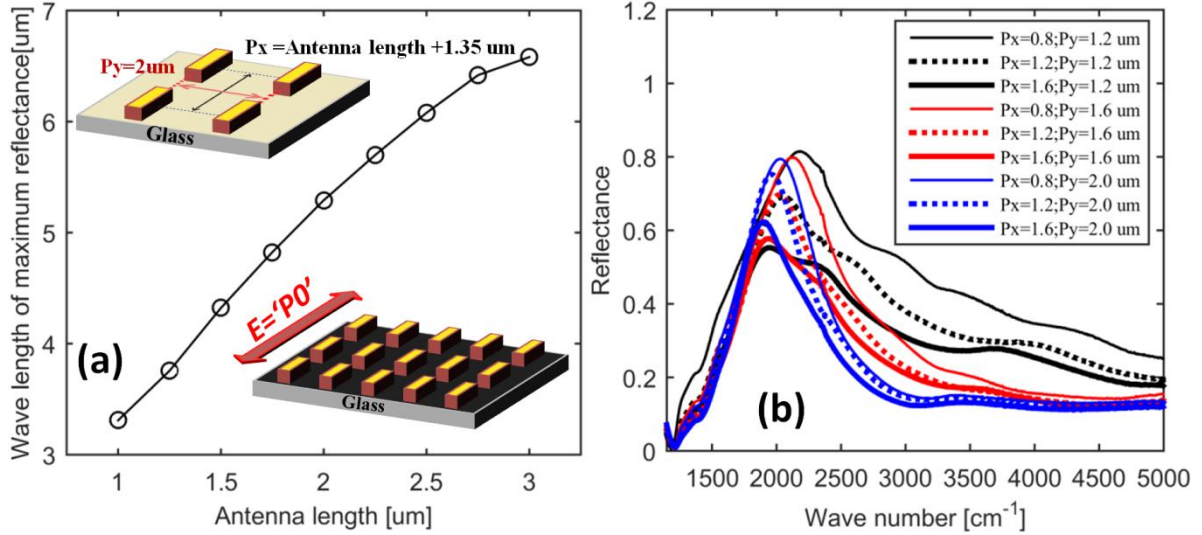
Figure 4: Reflectance dependence of antenna length and array spacing. a) Wavelength of maximum reflection signal as function of antenna length (L) for Px=L+1.35µm, and Py=2µm. The top and bottom insets illustrate the spacing between neighbouring antennas and the orientation of the electric field vector of the probing light. **b)** Reflectance curves for 2µm long antennas for 'P0' polarization at different spacing, as indicated in the legend.

Next, we tested the performance of the nano-antennas arrays in SEIRA sensing application. The arrays of nano-antennas on glass substrate and a reference gold sample were coated with ~40 nm of PMMA. PMMA is known for having several characteristic absorption fingerprints at the spectral region that overlaps the electro-magnetic resonance of our fabricated structures[12,28]. The presence of PMMA can be observed in the form of strong Fano-like dip at in the FTIR reflectance spectra at **1730** cm^{-1} (due to C=O stretching in the PMMA molecules) for polarized probing light with electric-field along the antenna ('P0' in figure 5a), but is barely distinguishable for the transverse polarization ('P90') or the planar Au layer (figure 5b). To distinguish between the broad resonance of the antennas and vibration modes in the reflectance curve, a running-average of 30 points was subtracted from each of the curves, similar to the technique of [12]. This allowed us to better identify additional vibrational modes typical to PMMA[12,28]: absorption peaks at **2950** (due to CH_3 asymmetric stretching), bands at **1440-1485** cm^{-1} (due to CH_2 scissoring and CH_3 deformation), peak of **1390** cm^{-1} (due to OCH_3 deformation), bands appearing at **1260–1270** cm^{-1} (corresponding with C–O stretching), and at **1190** cm^{-1} (attributed to CH_2 twisting).
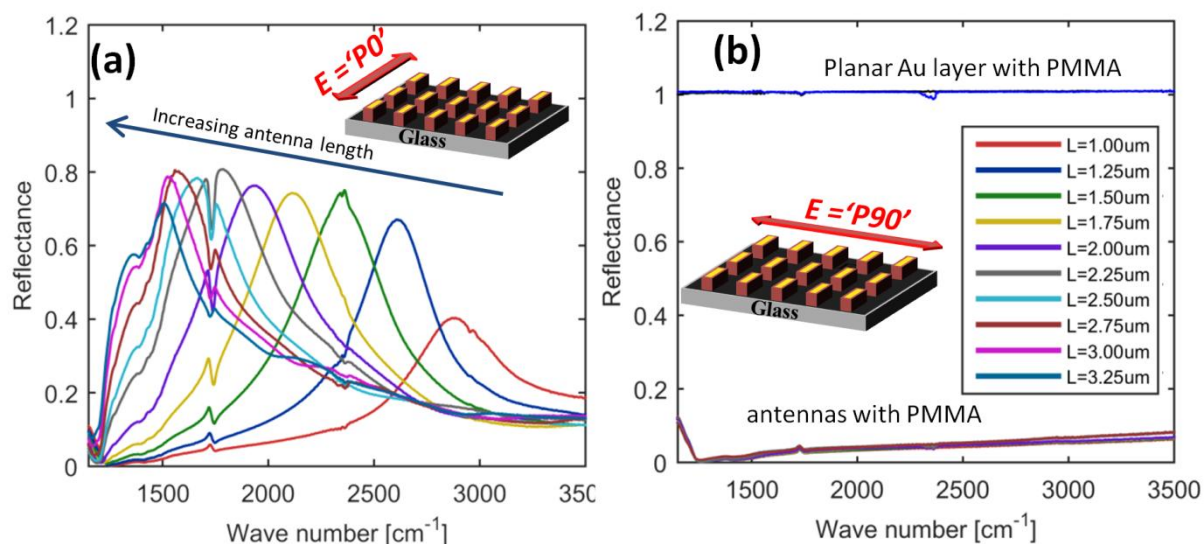
Figure 5: Absorption signal of PMMA – FTIR reflectance curves of antennas (L=1.0 to 3.25µm; Px=L+0.95µm; Py=2.0µm) and planar Au layer covered with 40nm of PMMA. a) probing light with polarized electric-field along the long axis of the antennas; b) Probing light with polarized electric-field transverse the antennas, and reflectance spectra of the planar Au reference sample. Insets illustrate the orientation of the electric field vector of the probing light.

The importance of been able to tune the antenna resonance (e.g. by varying its length, and/or the array parameters) is exhibited in Figure 6 and 7. Figure 6a presents the analyzed data for antennas of various lengths and fixed array parameters (Px=L+0.95µm; Py=2.0µm) for the two probing light polarizations and a planar 50 nm sheet of gold. The 1730 cm^{-1} absorption peak in this figure is strongest for antennas with intermediate length of 2.25µm; however, the 2950 cm^{-1} peak (no.8) is not apparent for these antenna lengths, and can only be detected with short antennas (L<1.25µm) which resonate at shorter wavelengths. Following the same trend, some of the peaks at wave-numbers smaller than 1500 cm^{-1} (peaks no. 2-7) only appears for long antennas with red-shifted resonance. Figure 7 presents the enhancement factors as function of antennas length for the same for the 8 absorption peaks and arrays of figure 6a. (where the enhancement factor is defined as the difference between the local minima and maxima of the absorption peaks, normalized relative to the difference between the local minima and maxima of the planar Au layer). The evolution of the enhancement factors as function of antenna length for the different absorption peaks demonstrates the importance of matching the LSPR of the antennas to the absorption peak. For example, the 2950 cm^{-1} peak is maximally enhanced for the 1µm long antenna with LSPR of about 2870 cm^{-1} (Figure 5a), and is decreasing rapidly for longer antennas; the 1730 cm^{-1} peak is maximally enhanced with antennas with LSPR of 1780 cm^{-1}; a similar trend is found for the other peaks, with maximum enhancement at longer antennas length as the absorption peaks are red-shifted. For transverse polarization ('P90'), the enhancement is practically invariant of antenna length with enhancement factors similar to the planar gold film.
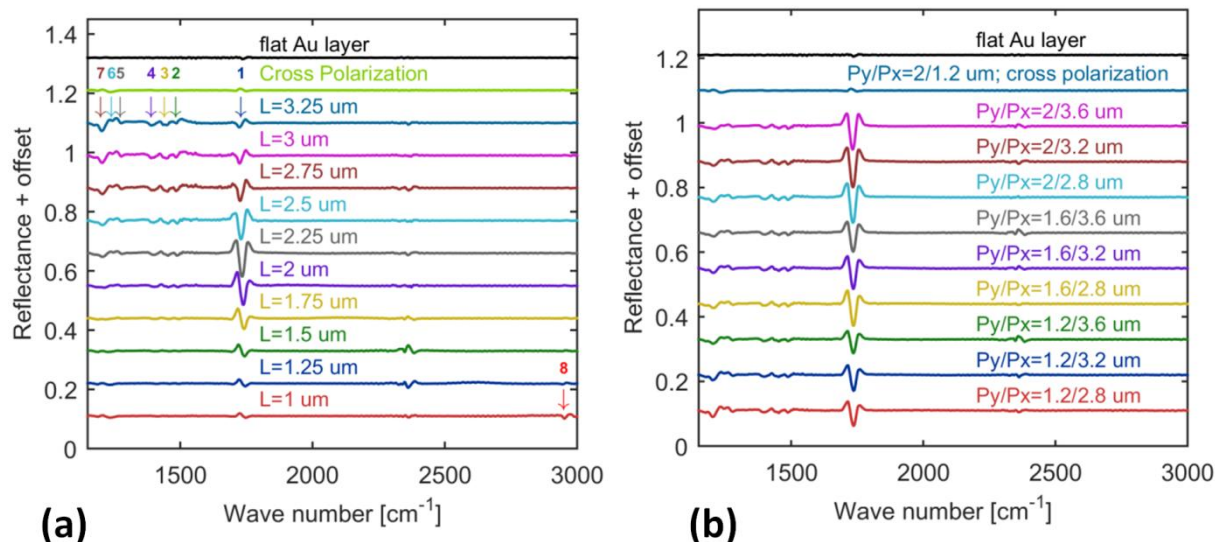
Figure 6: Analyzed data of FTIR reflectance curves of antennas and planar Au layer covered with 40 nm of PMMA. The running average (30 points) of the measured reflection curves was subtracted from the same measured data. The arrows labelled from 1 to 8 indicate typical vibrational modes of PMMA at 1730, 1485,1440, 1390,1275, 1240, 1200, and 2950 cm^{-1}. a) For of antennas with varying length and fixed array spacing: Px=L+0.95µm; Py=2.0µm. b) For fixed antennas length L=2.25µm and varied array spacing as indicated in the plot. For both plots, unless stated otherwise, probing light was with polarized electric-field along the long axis of the antennas ('P0'). The absorption signal at 2350 cm^{-1} is attributed to atmospheric CO_2 and is notably affected by the breathing of the FTIR operator.
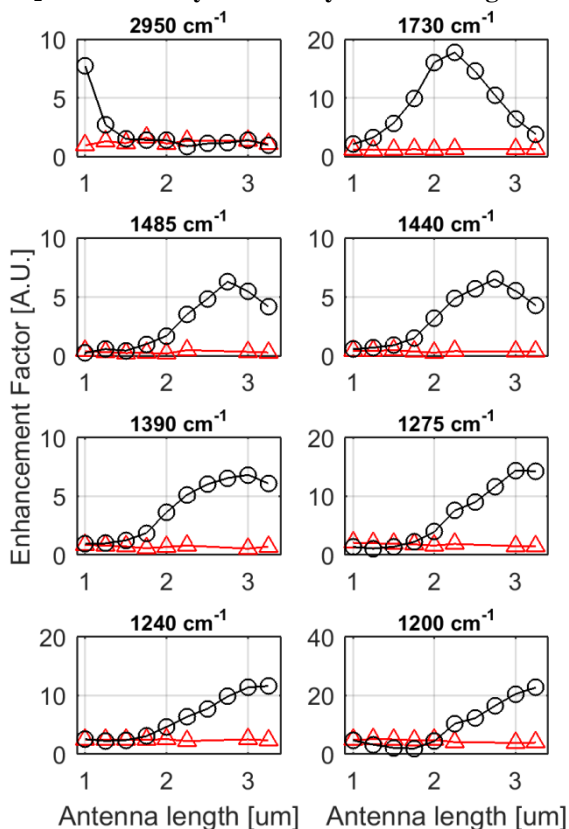

Figure 7: Enhancement of the absorption peaks as function of antenna length. The black circles (red triangles) are for probing light with polarized electric-field along (transverse) the long axis of the antennas. note the different scale for the different peaks.

The optical measurements presented heretofore were of Au antennas fabricated on glass substrate using the 'through glass' approach. In these structures, the dispersion of the glass substrate (i.e. strong

reflection for wave numbers smaller than 1250 cm^{-1}) suppresses long wavelength plasmonic resonances and prevented enhancement of the molecular vibration signal at wave numbers lower than ~1200cm^{-1}. In order to extend the range at which molecular sensing is achievable, arrays of nano-antennas were fabricated on Si substrate using the 'through-coverslip' approach (fig 1c). Figure 8. presents the FTIR reflection spectra of Au antennas on Si substrates before (figure 8a) and after (figure 8b) coating with thin layer of PMMA. The use of Si substrates revealed additional vibrational mode at 1140 cm^{-1} (C-O-C stretching[12]) with maximal enhancement factor of 5.7 for 1.45µm long antenna, and in principle enables in our system the identification of molecular fingerprints up to 600cm^{-1} (figure 9). The analysis of the evolution of the enhancement factor as function of antenna length for the Si substrate is provided in the supplementary material.
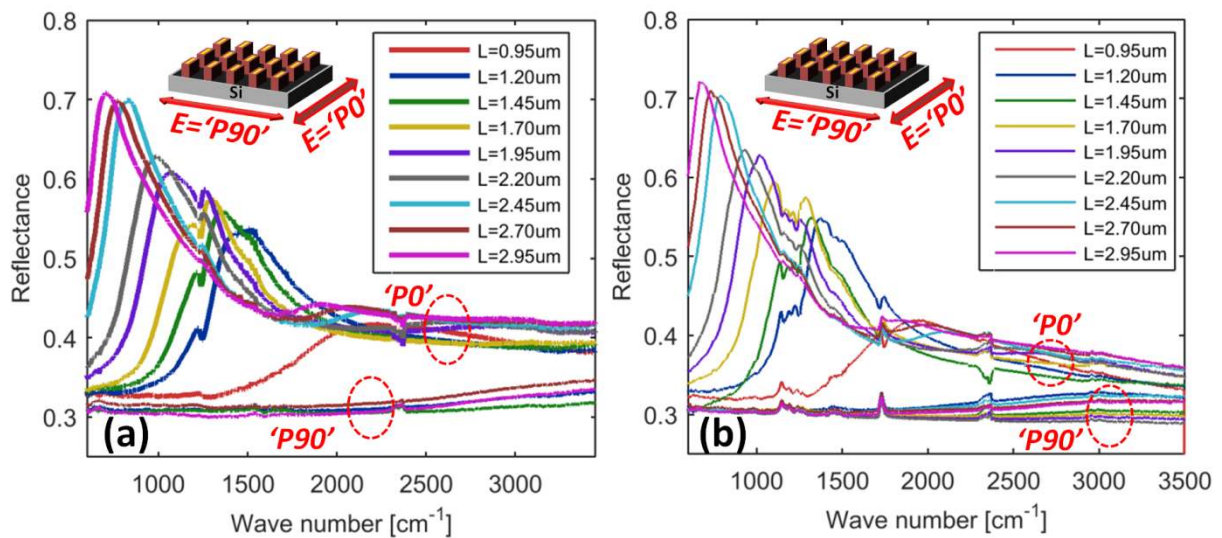

Figure 8: FTIR reflection measurements of Au antennas arrays on Si substrate, normalized relative to the reflectivity of gold. The two polarizations of the electrical field of the probing light are indicated in the inset. (a) bare antennas. (b) Antennas covered with 80nm of PMMA. In both graphs the pitch distance along and transverse the antennas were Px=L+1.20µm and Py=2.0µm, respectively.
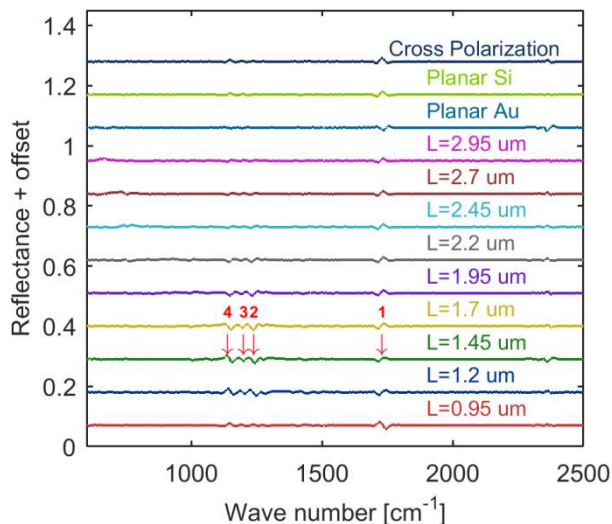

Figure 9: Analyzed data of FTIR reflectance curves of Au antennas on Si substrates, covered with 80 nm of PMMA. The running average (30 points) was subtracted from the measured FTIR reflectance. Array spacing is fixed at Px=L+1.2µm; Py=2.0µm. The arrows labelled from 1 to 4 indicate typical vibrational modes of PMMA at 1730, 1240, 1200, and 1140cm^{-1}, respectively. Unless indicated otherwise, the electrical field of the probing light was polarized along the antennas ('P0').

In order to test the speed of the writing of mm-scale devices, and their uniformity over large area, we fabricated 1mm x 1mm arrays of Au antennas using the through-glass approach (figure 10). The mm^2 arrays demonstrated uniform reflectivity over the whole area (inset of figure 10) with a writing time of 4min/mm^2 (for 2μm long Au antennas and Px=Py=4μm) – three times faster than the writing time of devices with similar array parameters written with single-beam research-level standard EBL system (eLINE, Raith, with 20μm aperture and 20kV beam). A ten-times increase in the throughput over such EBL systems may be achieved with better optimization of the writing parameters, as demonstrated in [16]. We emphasize the importance of writing-speed by noting that fast writing speed do not only enables a rapid research and development of new structures and devices, but it also enables the fabrication of mm-scale arrays (which obviate the need for probing the nano-structures via complicated microscopy, and improves the collection of light, hence signal to noise ratio) at reasonable time.

Finally, the flexibility in fabrication of antennas of different materials – ITO, Silver, Titanium and gold – is demonstrated in figure 11.
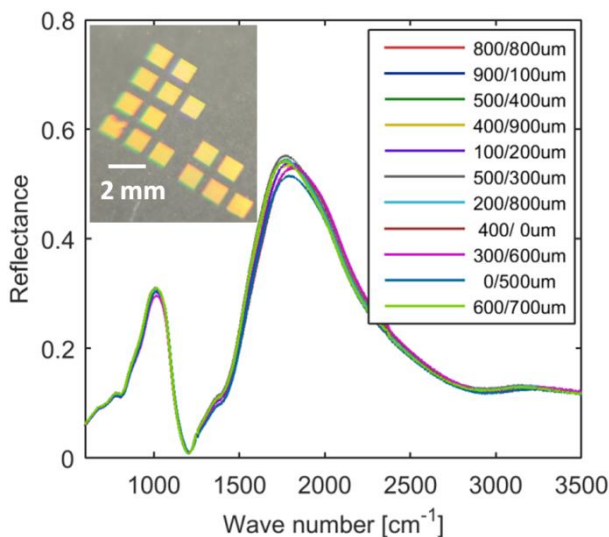

Figure 10: mm^2 arrays of nano-antennas. Inset: optical image of multiple 1x1 mm arrays. Main plot: FTIR reflectance spectra measured at different locations of a single mm^2 array. The legend indicates the position of the centre of the probed 100 x 100μm areas, measured in micrometres (along two orthogonal axes). from the corner of the 1mm^2 array.
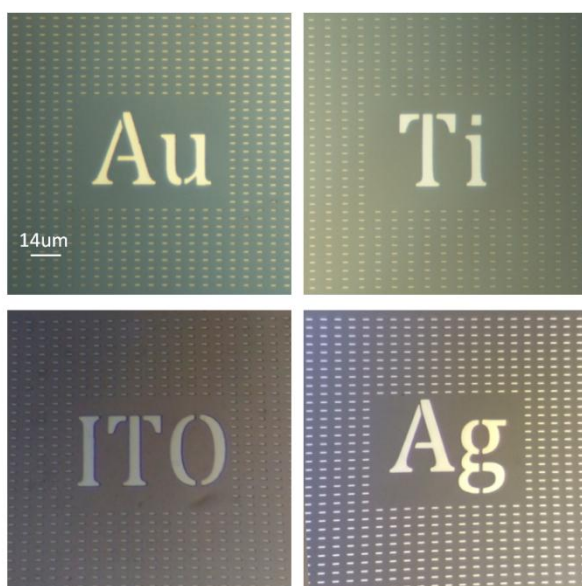
Figure 11: Optical microscopy images of arrays of nano-antennas made of different materials. From top-left clockwise: Gold (sputtered), Titanium (Sputtered), Silver (Thermally evaporated), and Indium-Tin-Oxide (In2O3/SnO2 90/10 WT%; sputtered). The nanostructures were fabricated on glass substrates using the 'through-glass' approach.

Conclusions

DLW lithography in positive-tone photo-resists followed by lift-off process offers a fast and flexible method for fabrication of arrays of nano-structures for surface-enhanced chemical sensing. The flexibility of this fabrication method, which enables a simple tuning of structures and arrays dimensions and antennas materials – allows capturing chemical fingerprints covering a wide spectral range in the Mid IR. A detection of molecular vibrational modes in a thin layer of PMMA deposited on gold nano-arrays written by DLW was demonstrated as an example for SEIRA sensing of analytes that could not be detected without the presence of the nano-structures. As DLW is gaining popularity as a powerful fabrication tool for flexible and accurate manufacturing of micro-fluidic channels and cells for various applications including sensing, the DLW lithography of the *active* sensing region presented in this paper enables a rapid and flexible design and fabrication of sensing devices using a single nano-fabrication tool.

Supporting Information

The Supporting Information is available free of charge.
FTIR enhancement factors for: Si sample, and glass sample with thick layer of PMMA

Acknowledgments

References

(1)   Fleischmann, M.; Hendra, P. J.; McQuillan, A. J. Raman Spectra of Pyridine Adsorbed at a Silver Electrode. *Chem. Phys. Lett.* **1974**, *26*, 163–166.

(2)   Moskovits, M. Surface-Enhanced Spectroscopy. *Rev. Mod. Phys.* **1985**, *57*, 783–826.

(3)   Crookell, A.; Fleischmann, M.; Hanniet, M.; Hendra, P. J. Surface-Enhanced Fourier Transform Raman Spectroscopy in the near Infrared. *Chem. Phys. Lett.* **1988**, *149*, 123–127.

(4)   Le, F.; Brandl, D. W.; Urzhumov, Y. A.; Wang, H.; Kundu, J.; Halas, N. J.; Aizpurua, J.; Nordlander, P. Metallic Nanoparticle Arrays: A Common Substrate for Both Surface-Enhanced Raman Scattering and Surface-Enhanced Infrared Absorption. *ACS Nano* **2008**, *2*, 707–718.

(5)   Hartstein, A.; Kirtley, J. R.; Tsang, J. C. Enhancement of the Infrared Absorption from Molecular Monolayers with Thin Metal Overlayers. *Phys. Rev. Lett.* **1980**, *45*, 201–204.

(6)   Enders, D.; Pucci, A. Surface Enhanced Infrared Absorption of Octadecanethiol on Wet-Chemically Prepared Au Nanoparticle Films. *Appl. Phys. Lett.* **2006**, *88*, 184104.

(7)   Anker, J. N.; Hall, W. P.; Lyandres, O.; Shah, N. C.; Zhao, J.; Duyne, R. P. V. Biosensing with Plasmonic Nanosensors. *Nat. Mater.* **2008**, *7*, 442–453.

(8)   Neubrech, F.; Pucci, A.; Cornelius, T. W.; Karim, S.; García-Etxarri, A.; Aizpurua, J. Resonant Plasmonic and Vibrational Coupling in a Tailored Nanoantenna for Infrared Detection. *Phys. Rev. Lett.* **2008**, *101*, 157403.

(9)   Kundu, J.; Le, F.; Nordlander, P.; Halas, N. J. Surface Enhanced Infrared Absorption (SEIRA) Spectroscopy on Nanoshell Aggregate Substrates. *Chem. Phys. Lett.* **2008**, *452*, 115–119.

(10)   Weber, D.; Albella, P.; Alonso-González, P.; Neubrech, F.; Gui, H.; Nagao, T.; Hillenbrand, R.; Aizpurua, J.; Pucci, A. Longitudinal and Transverse Coupling in Infrared Gold Nanoantenna Arrays: Long Range versus Short Range Interaction Regimes. *Opt. Express* **2011**, *19*, 15047.

(11)   Hoang, C. V.; Oyama, M.; Saito, O.; Aono, M.; Nagao, T. Monitoring the Presence of Ionic Mercury in Environmental Water by Plasmon-Enhanced Infrared Spectroscopy. *Sci. Rep.* **2013**, *3*, 1175.

(12)   Abb, M.; Wang, Y.; Papasimakis, N.; de Groot, C. H.; Muskens, O. L. Surface-Enhanced Infrared Spectroscopy Using Metal Oxide Plasmonic Antenna Arrays. *Nano Lett.* **2014**, *14*, 346–352.

(13)   Brown, L. V.; Zhao, K.; King, N.; Sobhani, H.; Nordlander, P.; Halas, N. J. Surface-Enhanced Infrared Absorption Using Individual Cross Antennas Tailored to Chemical Moieties. *J. Am. Chem. Soc.* **2013**, *135*, 3688–3695.

(14)   Brown, L. V.; Yang, X.; Zhao, K.; Zheng, B. Y.; Nordlander, P.; Halas, N. J. Fan-Shaped Gold Nanoantennas above Reflective Substrates for Surface-Enhanced Infrared Absorption (SEIRA). *Nano Lett.* **2015**, *15*, 1272–1280.

(15)   Bagheri, S.; Giessen, H.; Neubrech, F. Large-Area Antenna-Assisted SEIRA Substrates by Laser Interference Lithography. *Adv. Opt. Mater.* **2014**, *2*, 1050–1056.

(16)   Bagheri, S.; Weber, K.; Gissibl, T.; Weiss, T.; Neubrech, F.; Giessen, H. Fabrication of Square-Centimeter Plasmonic Nanoantenna Arrays by Femtosecond Direct Laser Writing Lithography: Effects of Collective Excitations on SEIRA Enhancement. *ACS Photonics* **2015**, *2*, 779–786.

(17)   Li, Y.; Su, L.; Shou, C.; Yu, C.; Deng, J.; Fang, Y. Surface-Enhanced Molecular Spectroscopy (SEMS) Based on Perfect-Absorber Metamaterials in the Mid-Infrared. *Sci. Rep.* **2013**, *3*, 2865.

(18)   Cheng, F.; Yang, X.; Gao, J. Ultrasensitive Detection and Characterization of Molecules with Infrared Plasmonic Metamaterials. *Sci. Rep.* **2015**, *5*, 14327.

(19)   Wan, W.; Yang, X.; Gao, J. Strong Coupling between Mid-Infrared Localized Plasmons and Phonons. *Opt. Express* **2016**, *24*, 12367–12374.

(20) Chang, Y.-C.; Lu, S.-C.; Chung, H.-C.; Wang, S.-M.; Tsai, T.-D.; Guo, T.-F. High-Throughput Nanofabrication of Infra-Red and Chiral Metamaterials Using Nanospherical-Lens Lithography. *Sci. Rep.* **2013**, *3*, 3339.

(21) Fredriksson, H.; Alaverdyan, Y.; Dmitriev, A.; Langhammer, C.; Sutherland, D. S.; Zäch, M.; Kasemo, B. Hole–Mask Colloidal Lithography. *Adv. Mater.* **2007**, *19*, 4297–4302.

(22) Aksu, S.; Yanik, A. A.; Adato, R.; Artar, A.; Huang, M.; Altug, H. High-Throughput Nanofabrication of Infrared Plasmonic Nanoantenna Arrays for Vibrational Nanospectroscopy. *Nano Lett.* **2010**, *10*, 2511–2518.

(23) Deubel, M.; Freymann, G. von; Wegener, M.; Pereira, S.; Busch, K.; Soukoulis, C. M. Direct Laser Writing of Three-Dimensional Photonic-Crystal Templates for Telecommunications. *Nat. Mater.* **2004**, *3*, 444–447.

(24) Cao, H.-Z.; Zheng, M.-L.; Dong, X.-Z.; Jin, F.; Zhao, Z.-S.; Duan, X.-M. Two-Photon Nanolithography of Positive Photoresist Thin Film with Ultrafast Laser Direct Writing. *Appl. Phys. Lett.* **2013**, *102*, 201108.

(25) Stanley, R. Plasmonics in the Mid-Infrared. *Nat. Photonics* **2012**, *6*, 409–411.

(26) Rubin, M. Optical Properties of Soda Lime Silica Glasses. *Sol. Energy Mater.* **1985**, *12*, 275–288.

(27) Bagheri, S.; Zgrabik, C. M.; Gissibl, T.; Tittl, A.; Sterl, F.; Walter, R.; De Zuani, S.; Berrier, A.; Stauden, T.; Richter, G.; *et al.* Large-Area Fabrication of TiN Nanoantenna Arrays for Refractory Plasmonics in the Mid-Infrared by Femtosecond Direct Laser Writing and Interference Lithography. *Opt. Mater. Express* **2015**, *5*, 2625.

(28) Juneja, R.; Roy, I. Surface Modified PMMA Nanoparticles with Tunable Drug Release and Cellular Uptake. *RSC Adv* **2014**, *4*, 44472–44479.

For TOC only: